

## New Features of Electron Phase Space Holes Observed by the THEMIS Mission

L. Andersson,<sup>1</sup> R. E. Ergun,<sup>1,2</sup> J. Tao,<sup>1,2</sup> A. Roux,<sup>3</sup> O. LeContel,<sup>3</sup> V. Angelopoulos,<sup>4</sup> J. Bonnell,<sup>5</sup> J. P. McFadden,<sup>5</sup>  
D. E. Larson,<sup>5</sup> S. Eriksson,<sup>1</sup> T. Johansson,<sup>1</sup> C. M. Cully,<sup>6</sup> D. L. Newman,<sup>7</sup> M. V. Goldman,<sup>7</sup>  
K.-H. Glassmeier,<sup>8</sup> and W. Baumjohann<sup>9</sup>

<sup>1</sup>Laboratory for Atmospheric and Space Physics, University of Colorado, Boulder, Colorado 80309, USA

<sup>2</sup>Department of Astrophysical and Planetary Sciences, University of Colorado, Boulder, Colorado 80309, USA

<sup>3</sup>Centre d'étude des Environnements Terrestre et Planétaires, Velizy, France

<sup>4</sup>Institute of Geophysics and Planetary Physics, University of California, Los Angeles, California 90055, USA

<sup>5</sup>Space Sciences Laboratory, University of California, Berkeley, California, 94720, USA

<sup>6</sup>Swedish Institute of Space Physics, Uppsala, Sweden

<sup>7</sup>Center for Integrated Plasma Studies, University of Colorado, Boulder, Colorado 80309, USA

<sup>8</sup>TUBS, Braunschweig, D-38106, Germany

<sup>9</sup>Space Research Institute, Austrian Academy of Sciences, A-8042 Graz, Austria

(Received 17 March 2009; published 5 June 2009; corrected 23 July 2009)

Observations of electron phase-space holes (EHs) in Earth's plasma sheet by the THEMIS satellites include the first detection of a magnetic perturbation ( $\delta B_{\parallel}$ ) parallel to the ambient magnetic field ( $\mathbf{B}_0$ ). EHs with a detectable  $\delta B_{\parallel}$  have several distinguishing features including large electric field amplitudes, a magnetic perturbation perpendicular to  $\mathbf{B}_0$ , high speeds ( $\sim 0.3c$ ) along  $\mathbf{B}_0$ , and sizes along  $\mathbf{B}_0$  of tens of Debye lengths. These EHs have a significant center potential ( $\Phi \sim k_B T_e / e$ ), suggesting strongly nonlinear behavior nearby such as double layers or magnetic reconnection.

DOI: 10.1103/PhysRevLett.102.225004

PACS numbers: 94.05.Fg, 52.35.Sb, 94.30.ep, 94.30.ct

Electron phase-space holes (EHs) [1–3] are ubiquitous in space plasmas. Observations have been made in the plasma sheet [4], auroral zone [5–7], magnetosheath [8], magnetopause [9], bow shock transition region [10], and solar wind [11]. EHs can be described as BGK [12] structures [3,13] or modeled by small potential expansion [1,14]. Theoretical treatments on generation concentrate on the electron two-stream instability [15,16] and Bunemann instability [17]. Most importantly, EHs are associated with processes such as double layers [18–20] and magnetic reconnection [17,21,22] making EHs a reliable indicator of strongly nonlinear behavior in plasmas.

The observational characteristics of EHs have been reported in a number of articles [7,8,23]. They are detected as bipolar electric field signals ( $\delta E_{\parallel}$ ) parallel to  $\mathbf{B}_0$  [4–6]. The parallel scale sizes ( $L_{\parallel}$ , defined here as the distance between peaks in  $\delta E_{\parallel}$ ) are most often several electron Debye lengths ( $\lambda_D$ ) and the speeds ( $v_{\text{EH}}$ ) are near to, but often less than, the electron thermal speed ( $v_e$ ). The perpendicular scale sizes ( $L_{\perp}$ ) are comparable to  $L_{\parallel}$  in the low-altitude auroral region [23], whereas it has been reported that  $L_{\perp} \gg L_{\parallel}$  in most other space environments [7,8]. EHs are most often weak ( $e\Phi_0/k_B T_e \ll 1$ , where  $\Phi_0$  is the center potential,  $e$  is the electron charge, and  $T_e$  is the electron temperature). THEMIS observations largely support these earlier results.

Space-based measurements record a profile in time, so the derivation of  $\Phi$  and  $L_{\parallel}$  depends on the speed of the EH. The statistical characteristics described above relate to

“slow-moving” EHs. By “slow-moving”, we mean that the speeds of the EHs are derived from the time delay between the signals of two spatially separated electric field probes [7,23]. Most instruments are limited to measuring  $v_{\text{EH}} < \sim 1000$  km/s with this technique.

In this article, we present the first 3D observations of magnetic field perturbations caused by EHs including the detection of a  $\delta B_{\parallel}$  signal. We show that the perpendicular magnetic perturbation ( $\delta B_{\perp}$ ) is primarily caused by the motion of a quasiaelectrostatic EH. In other words,  $\delta B_{\perp}$  is consistent with the Lorentz transformation of  $\delta E_{\perp}$  [5,23]. If EHs are quasiaelectrostatic in their rest frame (see later discussion on the “rest” frame),  $\delta B_{\perp}$  and  $\delta E_{\perp}$  can be used to accurately determine their speed, particularly if they are “fast-moving” ( $>1000$  km/s) and, subsequently, accurately derive  $\Phi$  and  $L_{\parallel}$ . We also show that EHs with a detectable  $\delta B_{\parallel}$  have quite different characteristics than reported by earlier observations. They have large electric field amplitudes,  $\delta E \sim O(100$  mV/m), high speeds ( $v_{\text{EH}} > v_e$ ), large parallel sizes ( $L_{\parallel} > 10\lambda_D$ ), moderate to strong center potentials ( $e\Phi/k_B T_e \sim 0.5$ ), and elongated shapes ( $L_{\parallel} > L_{\perp}$ ). We suggest that  $\delta B_{\parallel}$  arises from the  $\delta E \times \mathbf{B}_0$  electron motion in the EH and that  $\delta B_{\parallel} \propto \Phi$ . These observations have a number of similarities to laboratory observations of elongated, high-speed holes associated with magnetic reconnection [22].

The observations are from the THEMIS mission [24], which has five identical satellites in highly eccentric orbits at low inclination with apogees that range from  $10R_E$  to

$30R_E$ . The satellites carry electron and ion analyzers [25], a three-axis electric field instrument (dc—8 kHz) [26], a dc magnetometer [27], and a search coil magnetometer [28].

Figure 1 presents five minutes of observations from THEMIS Probe A at  $\sim 10R_E$  from Earth's center. The top panel [Fig. 1(a)] displays a spectrogram of the electron differential energy flux as a function of energy (vertical axis) and time (horizontal axis). The energy flux is calculated from a set of two-dimensional, energy-angle measurements averaged over a satellite spin period ( $\sim 3$  s) [25]. Data from two detectors are combined. The lower-energy electrons ( $\sim 10$  eV to  $\sim 30$  keV) are measured by an electrostatic analyzer whereas the higher-energy electrons are detected by a solid state telescope. The lowest-energy electron fluxes ( $< 25$  eV) are spacecraft photoelectrons. The black trace overlying the spectrogram is  $T_e$  in eV based on the electrostatic analyzer data.

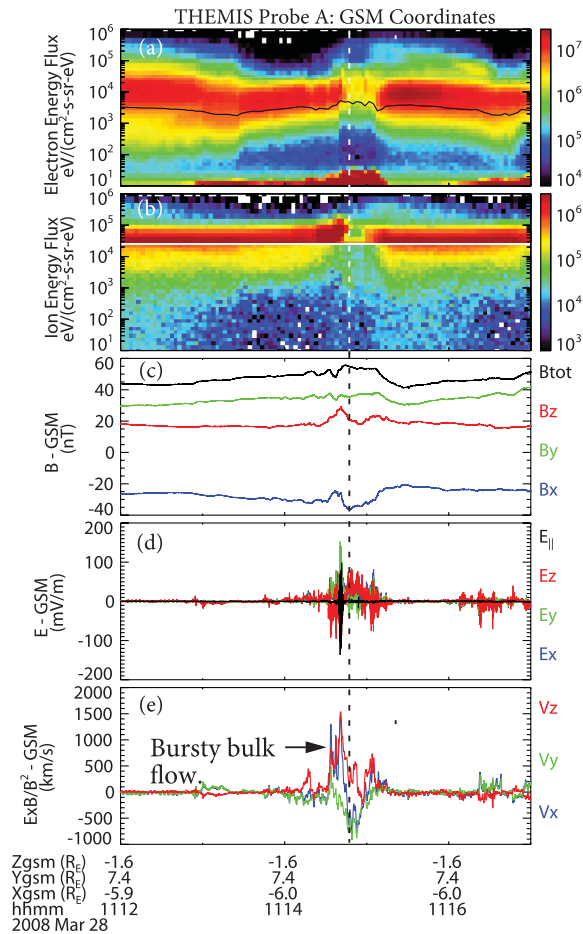


FIG. 1 (color). (a) Electron differential energy flux as a function of energy (vertical axis) and time (horizontal axis). The black trace is  $T_e$ . (b) Ion differential energy flux. (c) Magnetic field in GSM coordinates at 128 samples/s. The black trace is  $|\mathbf{B}_0|$ . (d)  $\mathbf{E}_0$  in GSM coordinates at 128 samples/s. The black trace is  $E_{0\parallel}$ . (e)  $\delta\mathbf{E} \times \mathbf{B}_0/|\mathbf{B}_0|^2$  low-pass filtered to 1 Hz in GSM coordinates. The vertical dashed line marks the period of the EHs in Fig. 2.

Figure 1(b) displays the differential energy flux of ions in the same format. A small gap in energy coverage is seen in the plot as white space. Figure 1(c) plots the dc-50 Hz magnetic field ( $\mathbf{B}_0$ ) at 128 samples/s in geocentric solar magnetospheric (GSM) coordinates. The absolute accuracy is better than 1 nT [27]. The color represents direction: blue is towards the Sun, red is near Earth's magnetic north, and green completes the set. The black trace in Fig. 1(c) is  $|\mathbf{B}_0|$ .

The dc-50 Hz electric field [ $\mathbf{E}_0$ , Fig. 1(d)] is measured by three orthogonal, dipole antennas [26]. The black trace in Fig. 1(d) represents the parallel electric field,  $E_{0\parallel}$ . The antennas in the spin plane of the spacecraft, mostly covering the GSM  $x$  and  $y$  directions, have  $\sim 40$  m and  $\sim 50$  m physical lengths and are accurate to approximately  $\pm 2$  mV/m, depending on plasma conditions. The spin-axis dipole, predominantly the GSM  $z$  direction, is  $\sim 7$  m and is accurate to  $\pm 20$  mV/m.

Figure 1(e) plots the quantity  $\mathbf{E}_0 \times \mathbf{B}_0/|\mathbf{B}_0|^2$  low-pass filtered to 1 Hz representing the flow perpendicular to  $\mathbf{B}_0$ . The  $x$ -component of the flow (towards Earth; blue trace) rises to over 1000 km/s at  $\sim 11:14.5$  UT indicating a bursty bulk flow event [29]. Such events are associated with magnetic reconnection occurring anti-Earthward of the spacecraft's position. During the bursty bulk flow event, the electron and ion energies increase [Figs. 1(a) and 1(b)] and  $\mathbf{E}_0$  and  $\mathbf{B}_0$  display strong variations [Figs. 1(c) and 1(d)].

Figure 2 presents 0.2 seconds of high-time resolution  $\delta\mathbf{E}$  and  $\delta\mathbf{B}$  signals (filtered from  $\sim 5$  Hz to  $\sim 3.3$  kHz; 8192 samples/s) during the time marked with a vertical dashed line in Fig. 1. The signals are in a magnetic coordinate system such that  $\delta E_{\parallel}$  is parallel to  $\mathbf{B}_0$ ,  $\delta E_X$  (accurate to  $\pm 2$  mV/m) is the perpendicular component measured only by the spin-plane booms, and  $\delta E_Y$  (accurate to  $\pm 20$  mV/m) completes the vector. The ac magnetic field signals are in the same coordinate system.

The  $\delta E_{\parallel}$  signal [Fig. 2(a)] shows a series of bipolar structures, a defining signature of EHs [4–6]. All of the EHs have a positive then negative polarity indicating that they are traveling in the same direction and, consequently, are likely to come from the same source. The perpendicular electric field signals [Figs. 2(c) and 2(e)] have a corresponding unipolar perturbation, again, typical of EHs. Some of the EHs are such that  $\delta E_X$  or  $\delta E_Y$  are greater than  $\delta E_{\parallel}$ , a sufficient but not necessary condition for  $L_{\parallel} \geq L_{\perp}$  (since the spacecraft may pass through the center of the EH rather than the edge, a small perpendicular signal does not, by itself, reveal the relation between  $L_{\parallel}$  and  $L_{\perp}$ ). Almost all of the EHs have a corresponding positive unipolar perturbation in  $\delta B_{\parallel}$  [Fig. 2(b)].

The perpendicular  $\delta\mathbf{E}$  and  $\delta\mathbf{B}$  signals [Figs. 2(c)–2(f)] are arranged in orthogonal pairs [ $\delta E_X$ , Fig. 2(c), is orthogonal to  $\delta B_Y$ , Fig. 2(d), etc.].  $\delta E_X$  and  $\delta B_Y$  are well correlated and  $\delta E_Y$  and  $\delta B_X$  have a negative correlation,

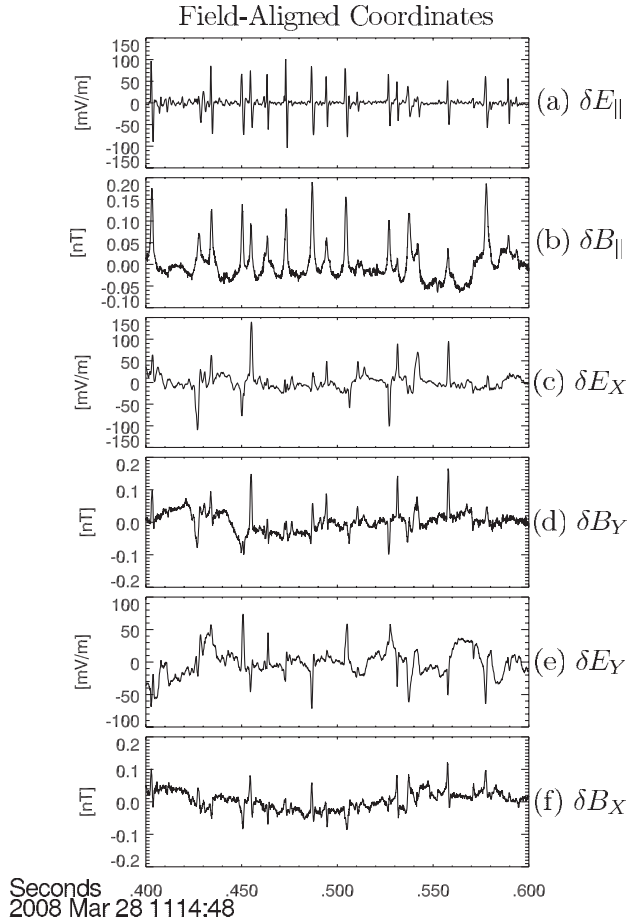


FIG. 2. (a)  $\delta E_{\parallel}$  (5 Hz–3.3 kHz) at 8192 samples/s during the period marked on Fig. 1. (b)  $\delta B_{\parallel}$  (5 Hz–3.3 kHz) at 8192 samples/s. (c)  $\delta E_X$  is from the long wire antennas and accurate to  $\pm 2$  mV/m. (d)  $\delta B_Y$  is orthogonal to  $\delta E_X$ . One can see that  $\delta E_X$  and  $\delta B_Y$  signals of EHs are well correlated. (e)  $\delta E_Y$  ( $\pm 20$  mV/m) is derived from a combination of all electric field dipole antennas including the short (7 m) dipole along the spacecraft spin axis [26]. (f)  $\delta B_X$ .

albeit somewhat weaker. These  $\delta \mathbf{E}$  and  $\delta \mathbf{B}$  signals are consistent with a Lorentz transformation of a moving quasiaelectrostatic structure ([30], changed to SI units):

$$\mathbf{B}' = \gamma(\mathbf{B} - \mathbf{v} \times \mathbf{E}/c^2) - \frac{\gamma^2}{1 + \gamma} \frac{\mathbf{v}(\mathbf{v} \cdot \mathbf{B})}{c^2}. \quad (1)$$

In their rest frame, the perpendicular  $\delta \mathbf{B}'$  signals nearly vanish. With  $\mathbf{v}_{\text{EH}}$  parallel to  $\mathbf{B}_0$ , the perpendicular components in Eq. (1) reduce to

$$\delta B_Y = \frac{v_{\text{EH}}}{c^2} \delta E_X, \quad \delta B_X = -\frac{v_{\text{EH}}}{c^2} \delta E_Y. \quad (2)$$

Most importantly, the data indicate that a quasiaelectrostatic frame exists. In other words, there is a frame in which the perpendicular  $\delta \mathbf{B}'$  signals nearly vanish (are minimum). The velocity of this frame, and presumably that of the EH,

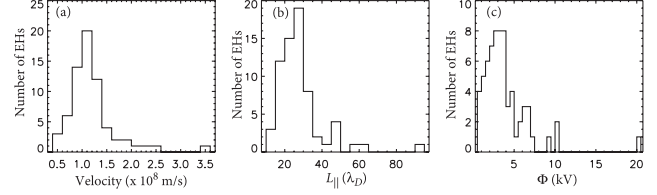


FIG. 3. (a) A histogram of the velocity of 67 EHs observed during a  $\sim 16$  s wave burst period (11:14:41 UT to 11:14:57 UT on March 28, 2008). The velocity was derived as  $c^2 \delta B_Y / \delta E_X$ . We note that one event has a derived speed greater than  $c$  which is either due to the uncertainty in  $\delta B_Y$  and  $\delta E_X$  or a strong electromagnetic ( $\delta B_r$ ) contribution. (b) A histogram of the parallel size of the EHs.  $L_{\parallel}$  is the distance between the negative and positive peaks in  $\delta E_{\parallel}$  assuming the EH is traveling at the derived velocity. (c) A histogram of the potential of the EHs derived from the  $\delta E_{\parallel}$  signal. The spacecraft may not have passed through the center of the EH, so  $\Phi$  represents a lower bound.

can be derived from  $\delta E_X$  and  $\delta B_Y$ , the more accurate of the orthogonal pairs.

Figure 3(a) displays the derived velocity ( $c^2 \delta B_Y / \delta E_X$ ) of 67 EHs detected in a  $\sim 16$  s “wave burst” period (11:14:41 UT to 11:14:57 UT on March 28, 2008) of high-time resolution (8192 samples/s) waveform that includes the data in Fig. 2 (see Refs. [24,26] for discussion on wave burst data collection). The mean velocity of the EHs is  $\sim 1 \times 10^8$  m/s. This high speed implies that these EHs are traveling faster than the thermal velocity ( $v_e \sim 4 \times 10^7$  m/s). Using the derived velocity, the size of the EHs along  $\mathbf{B}_0$  is displayed in Fig. 3(b).  $L_{\parallel}$  is roughly  $30 \lambda_D$ , where  $\lambda_D \sim 3.0$  km (derived from a 3 s average electron distribution). The mean value of  $\Phi$  [Fig. 3(c)] is  $\sim 3$  keV. Within uncertainties,  $T_e \sim 8$  keV (parallel to  $\mathbf{B}_0$ ). We cannot determine the radial offset of the measurements (distance perpendicular to  $\mathbf{B}_0$  from the center of the EH), so  $\Phi$  represents a lower bound. These EH observations have moderate potentials ( $e\Phi/k_B T_e \sim 0.5$ ) and are unusual in that  $v_{\text{EH}} > v_e$ , and  $L_{\parallel}$  is tens of  $\lambda_D$ . Similar results were reported from laboratory experiments on magnetic reconnection [22].

The presence of the  $\delta B_{\parallel}$  signal supports the above conclusions. This signal can be explained from the electron  $\delta \mathbf{E} \times \mathbf{B}_0$  currents generated by the perpendicular electric field signal. In the spacecraft frame, the duration of the EHs ( $\sim 1.2$  ms) is about 2 times the electron gyro-period ( $\sim 0.66$  ms), so an electron drift can be established whereas the ion motion is negligible. The resulting perpendicular current loop is around the center of the EH with  $J_{\phi} \cong -en_e \delta E_r / |\mathbf{B}_0|$ . Here,  $\delta E_r$  represents the radial perpendicular electric field perturbation, and  $n_e$  is the ambient electron density. This current will generate a magnetic field in the same direction as  $\mathbf{B}_0$  in the center of the EH; hence,  $\delta B_{\parallel}$  is always positive. The amplitude of  $\delta B_{\parallel}$  depends on  $\delta E_r$  and the shape of the EH.



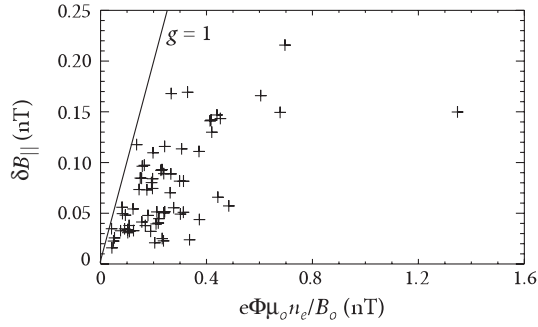


FIG. 4. The maximum value of  $\delta B_{\parallel}$  versus  $e\Phi\mu_0 n_e/B_0$  for the 67 EH measured in a 16 s burst period. There is no correction for radial offset, so both  $\delta B_{\parallel}$  versus  $\Phi$  represent lower bounds.  $\delta B_{\parallel}$  and  $\Phi$  do not have the same behavior as a function of radial offset, so the data exhibit significant scatter.

By modeling the hole as cylindrically symmetric with a Gaussian shape:

$$\Phi(r, z) = \Phi_0 e^{-r^2/2L_{\perp}^2} e^{-z^2/2L_{\parallel}^2}, \quad (3)$$

$\delta B_{\parallel}$  at the center of the EH can be derived by integrating the Biot-Savart equation:

$$\delta B_{\parallel}(r = 0, z = 0) = \frac{e\Phi_0\mu_0 n_e}{B_0} g(L_{\parallel}, L_{\perp}), \quad (4)$$

where  $g(L_{\parallel}, L_{\perp}) < 1$ , is a dimensionless geometric factor.

Figure 4 presents  $\delta B_{\parallel}$  versus  $e\Phi\mu_0 n_e/B_0$  for the 67 EHs measured in the 16 s wave burst period. We do not correct for radial offset ( $r \neq 0$ ), so both  $\delta B_{\parallel}$  and  $\Phi$  represent lower bounds.  $\delta B_{\parallel}$  and  $\Phi$  do not have the same behavior as a function of radial offset, so the data exhibit significant scatter. There are, however, two important properties. The values of  $\delta B_{\parallel}$  are nearly equal to but always less than that of  $e\Phi\mu_0 n_e/B_0$  consistent with  $g(L_{\parallel}, L_{\perp}) < 1$  and, furthermore,  $\delta B_{\parallel}$  increases with increasing  $\Phi$ . These data, along with the observation that  $\delta B_{\parallel} > 0$ , support our supposition that  $\delta B_{\parallel}$  results from electron  $\delta \mathbf{E} \times \mathbf{B}_0$  currents. Thus the  $\delta B_{\parallel}$  signal is in consort with the large amplitudes, high speeds, moderate to strong potentials, and elongated shape of the EHs.

Since the  $\delta B_{\parallel}$  exists in all frames, the EHs cannot be entirely electrostatic. If an EH is cylindrically symmetric, then a radial magnetic field must be present, even in the rest frame ( $\delta B_r \neq 0$  since  $\nabla \cdot \mathbf{B} = 0$ ). The rest frame is best defined as the frame in which the azimuthal magnetic field vanishes.  $\delta B_r$  is due to  $J_{\phi}$ , so it should be detected by a spacecraft as bipolar signal (the radial magnetic field of a current ring has opposite signs for  $z > 0$  and  $z < 0$ ). Careful examination of the measured magnetic field signals in Fig. 2 show that they are predominantly unipolar, so  $\delta B_r \ll \delta B_{\parallel}$ .  $\delta B_r$  is expected to be small if  $L_{\parallel} \geq L_{\perp}$ . A small  $\delta B_r$  is consistent with the elongated shape.

In conclusion, we have presented observations of the perturbation magnetic field and the first report of  $\delta B_{\parallel}$

associated electron phase-space holes. These EHs differ from earlier observations in that they have high speeds ( $v_{EH} > v_e$ ), large parallel sizes ( $L_{\parallel} > 10\lambda_D$ ), significant center potentials ( $e\Phi/k_B T_e \sim 1$ ), and elongated shapes ( $L_{\parallel} > L_{\perp}$ ). In particular, these EHs have many characteristics that are similar to those generated by magnetic reconnection in a laboratory experiment [22]. EHs also are known to be generated by double layers [18–20], so observations of EHs are an indicator of nonlinear, kinetic behavior in the active plasma sheet.

This work was supported by data analysis grants from NASA and German DLR for THEMIS and NASA support for the Fast Auroral Snapshot Explorer. The authors wish to thank the entire THEMIS team.

- [1] H. L. Berk, C. E. Nielsen, and K. V. Roberts, *Phys. Fluids* **13**, 980 (1970).
- [2] H. Schamel, *Plasma Phys.* **14**, 905 (1972).
- [3] V. A. Turikov, *Phys. Scr.* **30**, 73 (1984).
- [4] H. Matsumoto *et al.*, *Geophys. Res. Lett.* **21**, 2915 (1994).
- [5] R. E. Ergun *et al.*, *Geophys. Res. Lett.* **25**, 2041 (1998).
- [6] R. E. Ergun *et al.*, *Phys. Rev. Lett.* **81**, 826 (1998).
- [7] J. R. Franz, P. M. Kintner, and J. S. Pickett, *Geophys. Res. Lett.* **25**, 1277 (1998).
- [8] J. S. Pickett *et al.*, *Nonlinear Proc. Geophys.* **10**, 3 (2003).
- [9] C. Cattell *et al.*, *Geophys. Res. Lett.* **29**, 1065 (2002).
- [10] S. D. Bale *et al.*, *Geophys. Res. Lett.* **25**, 2929 (1998).
- [11] A. Mangeney *et al.*, *Ann. Geophys.* **17**, 307 (1999).
- [12] I. B. Bernstein, J. M. Greene, and M. D. Kruskal, *Phys. Rev.* **108**, 546 (1957).
- [13] L. Muschietti, R. E. Ergun, I. Roth, and C. W. Carlson, *Geophys. Res. Lett.* **26**, 1093 (1999).
- [14] M. V. Goldman, D. L. Newman, and A. Mangeney, *Phys. Rev. Lett.* **99**, 145002 (2007).
- [15] Y. Omura, H. Kojima, and H. Matsumoto, *Geophys. Res. Lett.* **21**, 2923 (1994).
- [16] M. V. Goldman, M. M. Oppenheim, and D. L. Newman, *Geophys. Res. Lett.* **26**, 1821 (1999).
- [17] J. F. Drake *et al.*, *Science* **299**, 873 (2003).
- [18] R. E. Ergun *et al.*, *Phys. Rev. Lett.* **87**, 045003 (2001).
- [19] L. Andersson *et al.*, *Phys. Plasmas* **9**, 3600 (2002).
- [20] D. L. Newman, M. V. Goldman, and R. E. Ergun, *Phys. Plasmas* **9**, 2337 (2002).
- [21] C. Cattell *et al.*, *J. Geophys. Res.* **110**, A01211 (2005).
- [22] W. Fox, M. Porkolab, J. Egedal, N. Katz, and A. Le, *Phys. Rev. Lett.* **101**, 255003 (2008).
- [23] R. E. Ergun *et al.*, *Nonlinear Proc. Geophys.* **6**, 187 (1999).
- [24] V. Angelopoulos, *Space Sci. Rev.* **141**, 5 (2008).
- [25] J. P. McFadden *et al.*, *Space Sci. Rev.* **141**, 277 (2008).
- [26] J. W. Bonnell *et al.*, *Space Sci. Rev.* **141**, 303 (2008).
- [27] H. U. Auster *et al.*, *Space Sci. Rev.* **141**, 235 (2008).
- [28] A. Roux *et al.*, *Space Sci. Rev.* **141**, 265 (2008).
- [29] W. Baumjohann, G. Paschmann, and H. Lüher, *J. Geophys. Res.* **95**, 3801 (1990).
- [30] J. D. Jackson, *Classical Electrodynamics* (Wiley, New York, 1998), p. 558.